

Tubular Enhanced Geodesic Active Contours for Continuum Robot Detection using 3D Ultrasound

Hongliang Ren and Pierre E. Dupont, *Fellow, IEEE*

Abstract—Three dimensional ultrasound is a promising imaging modality for minimally invasive robotic surgery. As the robots are typically metallic, they interact strongly with the sound waves in ways that are not modeled by the ultrasound system’s signal processing algorithms. Consequently, they produce substantial imaging artifacts that can make image guidance difficult, even for experienced surgeons. This paper introduces a new approach for detecting curved continuum robots in 3D ultrasound images. The proposed approach combines geodesic active contours with a speed function that is based on enhancing the “tubularity” of the continuum robot. In particular, it takes advantage of the known robot diameter along its length. It also takes advantage of the fact that the robot surface facing the ultrasound probe provides the most accurate image. This method, termed Tubular Enhanced Geodesic Active Contours (TEGAC), is demonstrated through ex vivo intracardiac experiments to offer superior performance compared to conventional active contours.

I. INTRODUCTION

Real-time Three-dimensional Ultrasonography (3DUS) has become available for clinical diagnostics and interventional tasks [1], [2]. Compared with MRI or CT, ultrasound imaging has a number of advantages, including affordability, portability, patient and clinician safety owing to its use of non-ionizing acoustic transducers and real-time 3D volumetric imaging at 20 frames per second. The real-time capability has enabled instrument navigation during interventional procedures, such as straight shaft detection in intra-cardiac surgery [3], [4], [5], liver biopsies [6], prostate brachytherapy [7], and concentric tube robots in cardiac surgery [8], [9]. The main drawbacks of ultrasonography in contrast to MR and CT imaging, however, are a lower spatial resolution and imaging artifacts. Thus, accurate robot detection is the key challenging problem in the 3D ultrasound image-guided minimally-invasive interventions [1], [2], [3], [4], [5].

As an example, Fig. 1 (a) depicts a concentric tube robot inserted in the left atrium of a porcine heart. This configuration reflects a typical procedure in which the robot enters the heart through the vasculature under ultrasound guidance and to perform intracardiac repairs. Fig. 1(b) shows the acquired 3D ultrasound images with the curved robot tip visible in the middle of left atrium and artifacts from the robot obscuring the contour of the right atrium. When the curved instrument is manipulated through various positions and orientations, the

This work was supported by the National Institutes of Health under grants R01HL073647 and R01HL087797. Hongliang Ren, Ph.D., hongliang.ren@childrens.harvard.edu and Pierre Dupont, Ph.D., pierre.dupont@childrens.harvard.edu are with the Department of Cardiovascular Surgery, Children’s Hospital Boston, Harvard Medical School, 300 Longwood Ave., Boston, MA, 02115 USA.

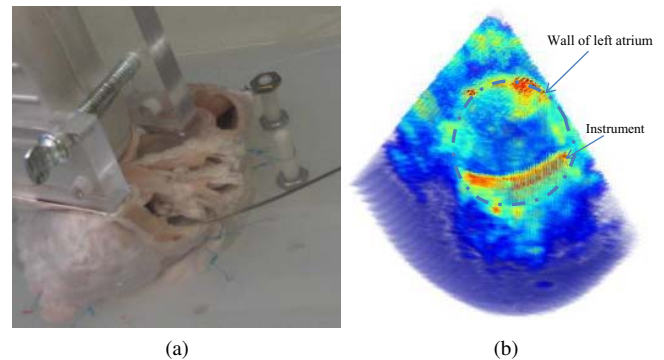


Fig. 1: Continuum robot inserted inside a porcine heart. (a) Experiment set up. (b) 3D ultrasound image showing both the left atrium and the curved robot.

artifacts also vary such that different portions of the robot and surrounding tissue are obscured.

This paper addresses the problem of instrument detection problem in 3D ultrasound in the presence of imaging artifacts. The proposed tubular enhanced geodesic active contour method addresses an essential step for improving robot visualization as well as for automation of surgical tasks in which the robot is directed to target locations using image-based localization.

The primary contribution of this article is the introduction of a novel tubular enhanced speed image to the active contour method for robot detection. The tubular enhanced speed image is formulated based on a new eigensystem analysis on the second-order image derivative and the prior observations of tubular imaging characteristics, i.e., known tubular diameter and discriminative tubular boundary contrast with respect to the transducer. While demonstrated here for robot detection, the intended application of this method is robot tracking. An additional contribution of this study is to provide a better understanding of the acquired 3DUS images, particularly, for visualizing the tubular instruments that can produce various significant artifacts.

The paper is organized as follows. Prior work related to 3D ultrasound image based instrument detection is reviewed in the next section. Section III presents the proposed algorithm for tubular enhanced geodesic active contours applied to continuum robot detection. In Section IV, the proposed approach is evaluated using ex vivo experiments. Conclusions appear in the final section.

II. RELATED WORK

For surgical robot detection in 3D ultrasound images, imaging artifacts can be a major challenge since there are many types of artifacts reflecting the various ways that ultrasound waves can interact with the robot. Previous studies in [10], [11], [4] have focused on detecting instruments with straight tool shafts using methods such as Principle Component Analysis (PCA) [10], Hough transforms [11] or Radon transform line detection [4]. These methods cannot be directly applied to detect curved robots and imaging artifacts were not directly addressed in these studies.

The main body of literature addressing artifacts focuses specifically on reducing speckle artifacts, which are widely present in ultrasound images due to the interference of sound waves with randomly distributed scatterers. Despeckling typically uses nonlinear filtering approaches such as median filtering or anisotropic diffusion [12]. There are also a few post-processing approaches to remove artifacts (such as those in Section IV) in 3D ultrasound and the filtering approaches have to be tailored to specific applications, to enhance or suppress particular structures.

A study of rod-like instrument imaging artifacts in 3D ultrasound has appeared in [13]. Four types of reverberation artifacts and two side-lobe artifacts were identified as major sources in 3DUS instrument imaging. The paper [13] also suggested appropriate ultrasound probe placement and instrument modifications for reducing artifacts. The artifacts described in [13] have been used to validate the method proposed here.

Active contour based detection methods have become powerful tools in medical image analysis [14], [15], particularly for boundary structure extraction, by applying local shape constraints to the contour evolution. A variety of approaches to active contour methods have been proposed and a good survey is [15]. Detection in cluttered, noisy images, as is the case in ultrasound detection of robots, suffers from a contour leakage problem due to the strong and varied imaging artifacts as shown in Section IV. Thus, it is necessary to apply new, specific constraints to guide contour evolution.

To address this problem, this paper aims at tailoring geodesic active contours to continuum robot detection in 3DUS by introducing both the tubularity of known diameter and the imaging characteristic of a clearer tubular boundary facing to the ultrasound probe.

III. METHODS AND MATERIALS

A. Algorithm Overview

In our prior work [9], a two-stage spatial circular parameter estimation method was proposed for estimating the configuration of a continuum robot in image coordinates. The volumetric image pre-processing pipeline proposed in that paper consisted of thresholding, connected component analysis and skeletonization to delineate the tubular robot object.

The block diagram in Fig. 2 outlines the overall working flow of the proposed Tubular Enhanced Geodesic Active Contour (TEGAC) algorithm. In the context of our earlier work in

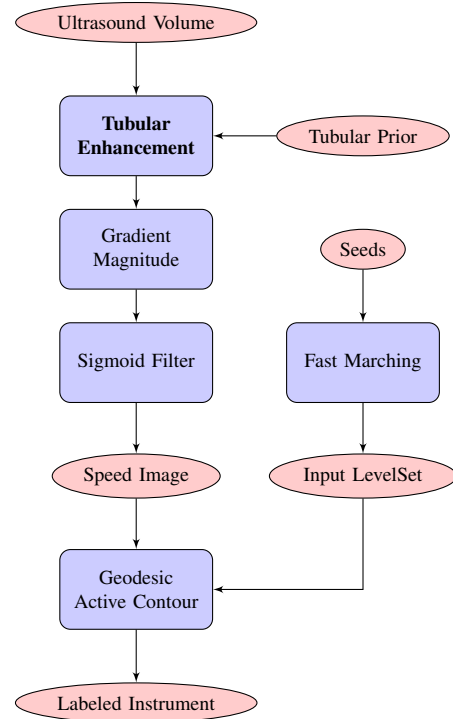


Fig. 2: Block diagram of the Tubular Enhanced Geodesic Active Contour (TEGAC) algorithm

[9], TEGAC is intended to replace the pre-processing pipeline. By incorporating the characteristics of 3D ultrasound imaging artifacts and the robot tubular prior information, TEGAC is more robust for robot detection in a cluttered environment. For robot detection, the initial seed is placed manually. For tracking, the labeled robot from TEGAC can serve to seed the subsequent volumetric frame. The labeled robot can also be used for two-stage spatial curvature parameter estimation [9].

A gray-level ultrasonic volume image, I , is defined as an $M \times N \times P$ matrix, where $I(i, j, k)$ represents the intensity of the voxel at the i th row, j th column, and k th slice, in the image volume space, which corresponds to Cartesian coordinates, $\mathbf{x} = (x, y, z)^T$, of the ultrasound transducer system, in the physical space. Here, x represents increasing azimuth, y represents increasing elevation and z indicates increasing distance from the transducer.

The active contour model has been used to delineate an object contour from a noisy image by minimizing an energy function associated with the given contour \mathcal{C} . Geodesic active contours, derived in [14], reduce the traditional energy-based active contour to the following equivalent intrinsic minimization problem:

$$\min_{\mathcal{C}(q)} \int g(|\nabla I(\mathcal{C}(q))|) |\mathcal{C}'(q)| dq, \quad (1)$$

where $g(\cdot)$ is a image-dependent speed function that controls the evolution speed of the active contour. The formulated speed function applies positive speed to the active contour in the homogeneous image regions and near zero speed when

approaching the object boundaries. A typical approach to formulate the speed term is to associate it with the image gradient or an alternate edge mapping. For example, the speed image used in [14] is computed directly from an edge mapping function related to the image gradient magnitude and is followed by a sigmoid filter. In 3D ultrasound robot images, this approach is inadequate since the boundary information is degraded by the various imaging artifacts, as illustrated in Section IV.

For curved continuum robot detection in 3D ultrasound volumes, the following two important tubular prior observations are useful for formulating a speed function. First, the diameters of the robot's sections are known along its length. Second, the robot surface facing the transducer produces the clearest boundary, whereas the surface facing away from the transducer is typically blurred. Starting from the detectable clearer boundary of the tubular structure and incorporating the known tubular diameter information, we can estimate the entire tubular location even it is blurred or cluttered, as described below.

B. Tubular Enhancement Module

The objective of the tubular enhancement module is to emphasize the tubular structure while suppressing the other non-tubular structures in the 3D ultrasound image. The approach is based on the analysis of the eigensystem of the image volume's Hessian matrix [16]. Let σ denotes the image scale of the analysis and $I_\sigma = I * G$, is the image convolved with a 3D Gaussian kernel $G(\mathbf{x}, \sigma) = 1/(2\pi\sigma^2)^{\frac{3}{2}} \exp(-(\mathbf{x}^T \mathbf{x})/2\sigma^2)$. Let ∇I_σ and $\mathcal{H}(I_\sigma)$ denote the gradient vector and Hessian matrix in the scale space σ .

The Hessian matrix is a second order vector field, i.e., the gradient of the image gradient, of an image at scale σ ,

$$\mathcal{H}(I_\sigma) = \nabla^2 I_\sigma = \sigma^{2\gamma} \frac{\partial^2 I_\sigma}{\partial x_i \partial x_j}, \quad (2)$$

where

$$\frac{\partial^2}{\partial x_i \partial x_j} = \begin{bmatrix} \frac{\partial^2}{\partial x_1^2} & \cdots & \frac{\partial^2}{\partial x_1 \partial x_n} \\ \vdots & \ddots & \vdots \\ \frac{\partial^2}{\partial x_n \partial x_1} & \cdots & \frac{\partial^2}{\partial x_n^2} \end{bmatrix},$$

γ is the commonly used scale normalization parameter and $n = 3$ for a 3D volume. For simplification, $\mathcal{H}(I_\sigma)$ at location \mathbf{x} and scale σ is represented as $\mathcal{H}_{\mathbf{x},\sigma}$ in what follows.

The eigensystem, including eigenvalues and eigenvectors, of the Hessian matrix reveals the geometrical dissimilarity of structures, based on the "vesselness" measure developed by [16]. Let $\lambda_1, \lambda_2, \lambda_3$ and $\mathbf{v}_1, \mathbf{v}_2, \mathbf{v}_3$ be the eigenvalues and corresponding eigenvectors of Hessian matrix, with increasing order of magnitude $|\lambda_1| \leq |\lambda_2| \leq |\lambda_3|$ and unit vector length $|\mathbf{v}| = 1$. Eigenvalue magnitude then corresponds to the intensity variance in the corresponding direction. Thus, \mathbf{v}_1 indicates the direction along the tubular structure with

minimum intensity variation and, for an idealized tube, $\lambda_1 \rightarrow 0$ while λ_2, λ_3 should be equally negative and large to represent the tubular cross-section.

Since the tubular surfaces facing the transducer are usually smoother and brighter, while the surfaces facing away from the transducer are blurred, it is useful to modify the vesselness measure. To do so, an additional term is introduced to emphasize the clearer probe-facing boundary by taking account of the boundariness and tubular diameter, corresponding to the image scale, σ , as defined by,

$$\mathcal{T}_{I,\sigma} = \begin{cases} 0, & \text{if } \lambda_2 > 0 \text{ or } \lambda_3 > 0 \\ (1 - e^{-\frac{A^2}{2a^2}}) e^{-\frac{B^2}{2b^2}} (1 - e^{-\frac{|\lambda_1|^2}{2c^2}}) (1 - e^{-\frac{D^2}{2d^2}}). \end{cases} \quad (3)$$

Here, $\lambda = [\lambda_1, \lambda_2, \lambda_3]^T$, $A = |\lambda_2/\lambda_3|$ for distinguishing plate and line structures, $B = |\lambda_1|/\sqrt{|\lambda_2\lambda_3|}$ for distinguishing tubular structures from blob structures, a, b, c, d are the coefficients to control the weights of A, B, C, D , and the first three terms containing a, b, c are those of the original vesselness function in [16]. The parameter D accounts for the normalized boundariness corresponding to the principal curvature of the Hessian matrix, as given by,

$$D = |\nabla I_\sigma(\mathbf{x} + \sigma \mathbf{v}_3)|$$

where \mathbf{v}_3 represents the direction corresponding to the maximum eigenvalue of the Hessian matrix.

C. Tubular Enhanced Active Contour Model

The results from the tubular enhancement module are used to formulate a speed function that guides the active contour evolution. In order to get an edge potential image to control the contour evolution speed, the speed function for the geodesic active contour model is formulated by passing the tubular enhanced images through a sigmoid filter,

$$g(\mathcal{T}_{I,\sigma}) = \frac{1}{1 + (\frac{n\|\nabla \mathcal{T}_{I,\sigma}\|}{\max\|\nabla \mathcal{T}_{I,\sigma}\|})^m}, \quad (4)$$

where m, n are user-specified parameters to adjust the evolution speed. Thus, the resulting speed image, $g(\cdot)$, is now an edge strength based stopping function for contour evolution: slowing evolution near the boundary and speeding evolution in homogeneous regions.

Similar to the derivations in [14], the Euler-Lagrange equation associated with (1) is a contour evolution model:

$$\frac{\partial \mathcal{C}(t)}{\partial t} = g(\mathcal{T}_{I,\sigma}) \kappa \mathcal{N} - (\nabla g(\mathcal{T}_{I,\sigma}) \cdot \mathcal{N}) \mathcal{N}, \quad (5)$$

and the associated level-set embedding function, ϕ , of the curve, \mathcal{C} , can be updated by,

$$\frac{\partial \phi}{\partial t} = g(\mathcal{T}_{I,\sigma}) \kappa \|\nabla \phi\| - \nabla g(\mathcal{T}_{I,\sigma}) \cdot \nabla \phi, \quad (6)$$

where $\mathcal{N} = \frac{\nabla \phi}{\|\nabla \phi\|}$ is unit normal to the curve, $\kappa = \text{div}(\frac{\nabla \phi}{\|\nabla \phi\|})$ is the curvature.

Therefore, by incorporating the tubular enhanced speed image, the contour represented by the zero level set of ϕ ,

is evolving according to three terms: 1) an image-dependent speed function pushing the contour to the tubular boundaries, 2) an internal smoothness term to minimize the curvature, and 3) an inflation force to expand or contract the contour.

IV. EXPERIMENTS

Two types of experiments were performed to validate the tubular enhancement based geodesic active contour (TEGAC) algorithm. First, the tubular enhancement module was evaluated in tank tests against the presence of various 3DUS imaging artifacts, in order to demonstrate the capability of generating effective speed images for the later steps. Second, the active contour evolution module was subsequently validated in ex vivo experiments in which a porcine heart is submerged in the water tank and the curved portion of the robot is placed inside the left atrium.

A. Materials and Setup

All experiments were performed in a water tank as shown in Fig. 1. Three dimensional ultrasound images were acquired using a Philips IE33 (www.philips.com) system with a 3D probe. The probe was mounted as shown in a linear stage while a piecewise constant curvature concentric tube robot [8] constructed from a superelastic NiTi alloy was submerged in the water. The bottom of the tank was lined with a rubber pad to reduce reverberation. The robot's distal section had a radius of curvature of $R_1 = 60$ mm, a diameter of 2 mm.

Standard settings of the imaging parameters were used during image generation, including 50% overall gain, 50% compression rate, frequency fusion mode 2, high density scan line spacing, 10 cm image depth, and zero dB power level. The resulting voxels have anisotropic spacing of $\{0.542$ mm, 0.706 mm, 0.451 mm $\}$ in the x , y and z directions, respectively.

B. Tubular Enhancement Filtering to Reduce Imaging Artifacts

Comet Tail Artifacts (CTA) and Tip Reverberation Artifacts (TRA), as indicated in Fig. 3, are prominent reverberation artifacts generated by multiple echoes when sound waves bounce back and forth between object interfaces with large differences in acoustic impedance. Such is the case for the interfaces between the water and the NiTi tubes. Each echo returning to the transducer is interpreted as a surface whose distance from the transducer corresponds to the return time.

Comet Tail Artifacts (CTA) show up as band-like structures and get stronger when the robot tube is orthogonal to the beam lines. For constant curvature tubes, the comet tail artifacts can arise all along the tube when the tube curvature is similar to beam curvature and the tube is placed conformal to the beam sector, as shown in Fig. 3. In the configuration of Fig. 3, each segment of the tube surface is close to a normal facing to the ultrasound probe, and the resulted CTA severely degrade imaging quality.

The proposed tubular enhancement is very effective at reducing CTA, as shown in Fig. 4, since these artifacts possess a plate-like pattern, which can be well distinguished from the

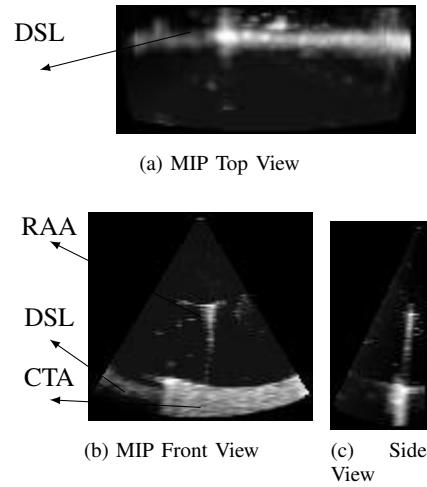


Fig. 3: Original image with artifacts: CTA, Comet Tail Artifacts; DSL, diffractive side lobe; and RAA, Range ambiguity artifacts. The images show 2D Maximum Intensity Projection (MIP) views for 3DUS volumetric images. (a) MIP Top View, (b) MIP Front View, (c) MIP Side View.

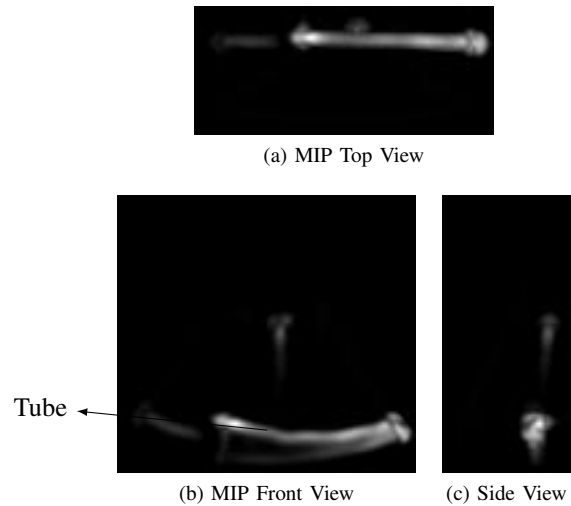


Fig. 4: Tubular enhancement filtering results in 2D Maximum Intensity Projection (MIP) views for 3DUS volumetric images. (a) MIP Top View, (b) MIP Front View, (c) MIP Side View.

tubular structure. Since the Tip Reverberation Artifact (TRA) also show ring-down effects, the tubular enhancement module can suppress most of the bank-like artifacts but less of the line-like artifacts as shown in Fig. 4.

Diffractive side lobe (DSL) artifacts are caused by off-axis peripheral waves. Since the edges and corners of a metallic robot are strong scatterers, the resulting reflections from the side lobes are strong enough to be detected by the transducer and misinterpreted as reflections arising from the main lobe of the transducer. This results in fictitious structures, such as shown in Fig. 3. Diffractive side lobe (DSL) artifacts can be partially reduced by the tubular enhancement module as shown

in Fig. 4. It works particularly well for artifacts far away from tip. For those close to the tip, however, the tubular structure of the artifacts makes them hard to distinguish from the robot itself.

Finally, range ambiguity artifacts (RAA) arise when the ultrasound beam undergoes multiple reflections of sufficient duration before returning to the probe that echoes from a prior pulse are misinterpreted as those from the most recent pulse. As can be seen from Fig. 3 and Fig. 4, range ambiguity artifacts can be suppressed to a certain degree, but cannot be fully removed. It can be noted, however, that this type of artifact is usually sufficiently far from the object being imaged that it can be excluded using prior configuration information.

C. Ex Vivo Experiments

It is more difficult to visualize robots inserted inside the body rather than in a water tank. To determine if the proposed algorithm is applicable to clinical situations, a porcine heart was submerged in the water tank and the concentric tube robot was inserted inside the left atrium, as shown in Fig. 1.

2D slice views of the robot are shown in Fig. 5 (a) and with the resulting overlaid TEGAC results in Fig. 5(b). The effect of tubular enhancement in comparison with the standard pre-processing of the geodesic active contour method is shown in Fig. 6. Given the same speed function parameters, $n = 0.088, m = 2$, the resulting speed images from the proposed TEGAC and conventional GAC methods are shown in Fig. 6 (a) and (b), respectively. These are applied to the active contour method for delineating the robot. The contour evolution model uses the same parameter set of inflation force, 1, curvature force, 0.2, advection force, 3.81 for the comparison. From the overlaid resulting contours, we can see that TEGAC can effectively evolve the contours to the object boundaries while the conventional GAC results in contour leakage owing to blurred edge information arising from artifacts. The leakage part can be clearly viewed in the rendered 3D model of Fig. 7 (a).

We tested the algorithm on a set of 20 ultrasound volumetric images containing the same robot and compared the results of the algorithm with those obtained through manual segmentation using the degree of volumetric overlap as computed with the DICE metric. It is defined as

$$DICE(A, B) = 2|A \cap B| / (|A| \cup |B|),$$

where A and B are two labeled volumetric structures to be compared. As plotted in Fig. 8, the average volumetric overlap metric for the 20 ultrasound volumes by TEGAC was 0.804 ± 0.0815 versus that by conventional Geodesic Active Contour (GAC) of 0.497 ± 0.087 . During the experiments, we observed that TEGAC can evolve to an accurate tubular shape representing the instrument, whereas the conventional GAC cannot accurately estimate the tubular boundaries. The resulting contour from GAC includes part of the artifacts and takes the shape of a curved elongated triangular prism, as partially shown in Fig. 7 (a).

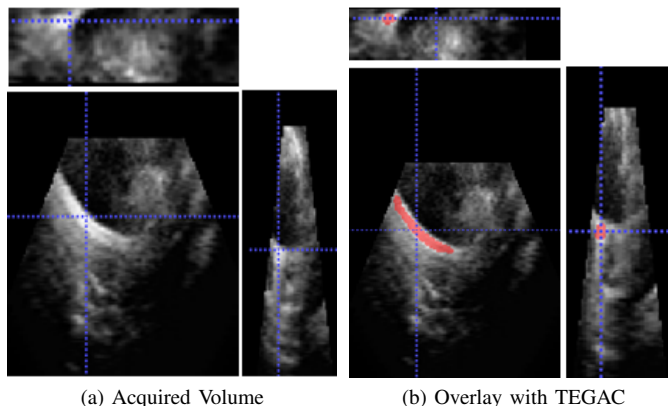


Fig. 5: Raw robot images and overlaid TEGAC results. The 2D slices correspond to front, top and side views. The crosshair locations indicate tubular object. (a) 2D slices of volumetric image. (b) 2D slices of volumetric image overlaid with the evolved contour from TEGAC.

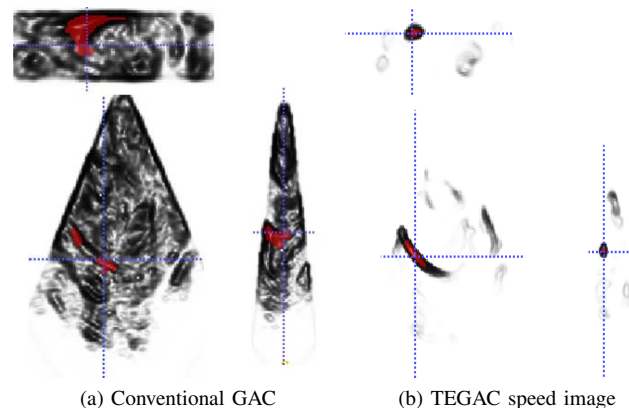


Fig. 6: Comparison between the conventional GAC and TEGAC algorithms. The 2D slices correspond to front, top and side views. The crosshair locations indicate tubular object. (a) Speed image overlaid with resulting active contour from conventional GAC; (b) Speed image overlaid with resulting active contour from TEGAC algorithm.

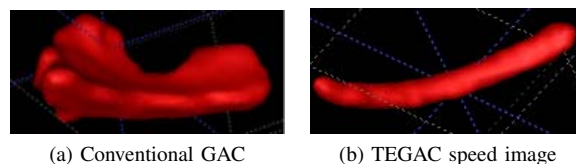


Fig. 7: 3D rendering of detected robot using conventional GAC and TEGAC algorithms. (a) Conventional GAC. (b) TEGAC algorithm.

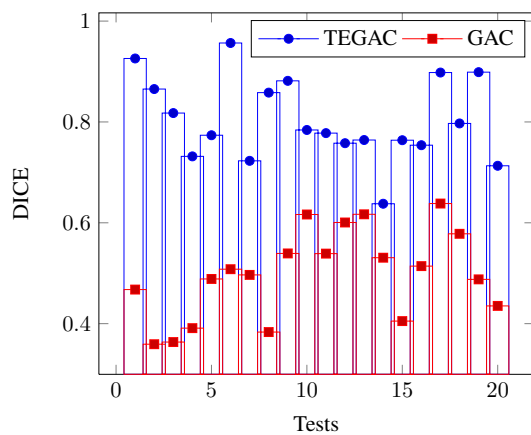


Fig. 8: DICE metric comparing manual segmentation, the TEGAC detection algorithm and the conventional Geodesic Active Contour (GAC) algorithm.

D. Discussion

The proposed TEGAC algorithm provides substantially improved results in comparison to standard geodesic active contours. The speed images produced by the proposed approach contain enhanced tubular structures at specific length scale corresponding to tube diameter. If the artifacts include ghost images of tubular structures with the same length scale, they will not be removed by the filter. In these situations, however, prior information on location can be incorporated to remove the ghost structures.

V. CONCLUSIONS AND FUTURE WORK

Motivated by the image guided robot navigation techniques of minimally invasive interventions, this paper has focused on developing techniques that leverage the underlying tubular geometry of continuum robots to ameliorate the effect of imaging artifacts on robot and tissue visualization using 3D ultrasound. Specifically, the proposed approach incorporates the prior characteristics of tubular robot imaging, including the clearer boundaries on the surface towards transducer, and the known diameter of robot tubes. This provides a new speed function for guiding the evolution of active contours.

As a next step, we plan to incorporate statistical prior shape information of the tubular continuum robots to further restrain contour evolution. We also plan to improve the computational speed by parallelizing the tubular enhancement algorithm for implementation on GPUs. Our long-term goals are to implement 3D ultrasound based tracking and servoing of continuum robots.

For the specific application of intracardiac interventions, the effect of heart motion on robot detection and tracking is an important future consideration. It is anticipated that heart motion will be beneficial in aiding robot tracking. This is substantiated by our observations during surgery that the robot is much easier to detect and track visually when viewing a sequence of volumes rather than a single volume.

ACKNOWLEDGMENT

The authors gratefully acknowledge the assistance of Scott Settlemier, Philips Medical Systems, and the useful discussions with colleagues Andrew Gosline, Panagiotis Vartholomeos and Genevieve Laing.

REFERENCES

- [1] J. Cannon, J. Stoll, I. Salgo, H. Knowles, R. Howe, P. Dupont, G. Marx, and P. del Nido, "Real-time three-dimensional ultrasound for guiding surgical tasks," *Computer aided surgery*, vol. 8, no. 2, pp. 82–90, 2003.
- [2] S. Yagel, S. M. Cohen, I. Shapiro, and D. V. Valsky, "3d and 4d ultrasound in fetal cardiac scanning: a new look at the fetal heart," *Ultrasound Obstet Gynecol*, vol. 29, no. 1, pp. 81–95, 2007. [Online]. Available: <http://dx.doi.org/10.1002/uog.3912>
- [3] J. Stoll and P. Dupont, "Passive markers for ultrasound tracking of surgical instruments," *Medical Image Computing and Computer-Assisted Intervention—MICCAI 2005*, pp. 41–48, 2005.
- [4] P. Novotny, J. Stoll, N. Vasilyev, P. Del Nido, P. Dupont, T. Zickler, and R. Howe, "GPU based real-time instrument tracking with three-dimensional ultrasound," *Medical Image Analysis*, vol. 11, no. 5, pp. 458–464, 2007.
- [5] S. Yuen, D. Kettler, P. Novotny, R. Plowes, and R. Howe, "Robotic motion compensation for beating heart intracardiac surgery," *The International Journal of Robotics Research*, vol. 28, no. 10, p. 1355, 2009.
- [6] E. M. Boctor, M. A. Choti, E. C. Burdette, and R. J. Webster III, "Three-dimensional ultrasound-guided robotic needle placement: an experimental evaluation," *The International Journal of Medical Robotics and Computer Assisted Surgery*, vol. 4, no. 2, pp. 180–191, 2008. [Online]. Available: <http://dx.doi.org/10.1002/rcs.184>
- [7] P. Yan, "MO-FF-A4-02: Automatic Shape-Based 3D Level Set Segmentation for Needle Tracking in 3D TRUS Guided Prostate Brachytherapy," *Medical Physics*, vol. 37, p. 3366, 2010.
- [8] P. Dupont, J. Lock, B. Itkowitz, and E. Butler, "Design and control of concentric-tube robots," *IEEE Transactions on Robotics*, vol. 26, no. 2, pp. 209–225, 2010.
- [9] H. Ren, N. V. Vasilyev, and P. E. Dupont, "Detection of curved robots using 3d ultrasound," in *IEEE/RSJ International Conference on Intelligent Robots and Systems*, in press, 2011.
- [10] J. Stoll, "Ultrasound-based navigation for minimally invasive medical procedures," Ph.D. dissertation, Boston University, 2007.
- [11] M. Ding, H. N. Cardinal, W. Guan, and A. Fenster, "Automatic needle segmentation in 3d ultrasound images," S. K. Mun, Ed., vol. 4681, no. 1. SPIE, 2002, pp. 65–76. [Online]. Available: <http://link.aip.org/link/?PSI/4681/65/1>
- [12] Q. Sun, J. A. Hossack, J. Tang, and S. T. Acton, "Speckle reducing anisotropic diffusion for 3d ultrasound images," *Computerized Medical Imaging and Graphics*, vol. 28, no. 8, pp. 461 – 470, 2004. [Online]. Available: <http://www.sciencedirect.com/science/article/B6T5K-4DM27VD-1/2/6d54ad59a19da796d4c39fe0b9890633>
- [13] J. Huang, J. K. Friedman, N. V. Vasilyev, Y. Suematsu, R. O. Cleveland, and P. E. Dupont, "Imaging artifacts of medical instruments in ultrasound-guided interventions," *J Ultrasound Med*, vol. 26, no. 10, pp. 1303–1322, 2007. [Online]. Available: <http://www.jultrasoundmed.org/cgi/content/abstract/26/10/1303>
- [14] V. Caselles, R. Kimmel, and G. Sapiro, "Geodesic active contours," *International Journal of Computer Vision*, vol. 22, no. 1, pp. 61–79, 1997.
- [15] S. Lankton and A. Tannenbaum, "Localizing region-based active contours," *IEEE Transactions on Image Processing*, vol. 17, no. 11, pp. 2029–2039, 2008.
- [16] A. Frangi, W. Niessen, K. Vincken, and M. Viergever, "Multiscale vessel enhancement filtering," *Medical Image Computing and Computer-Assisted Intervention MICCAI98*, pp. 130–137, 1998.